inter.noise 2014
MELBOURNE AUSTRALIA
16-19 NOVEMBER

Application of lattice Boltzmann method to research bubble interacting with spherical particle

Dongyan SHI[1]; Zhikai WANG[2]; Aman ZHANG[3]

[1] Harbin Engineering University, China

[2] Harbin Engineering University, China

[3] Harbin Engineering University, China

ABSTRACT

During the process of bubbles interacting with particles, the bubble movement velocity, jetting phenomenon, topological deformation, and even properties of flow field may demonstrate novel variation. To investigate these characteristics, the lattice Boltzmann method (LBM) which is based on kinetic theory is adopted to build up the three dimensional coupled model. The gas-liquid interface with large density ratio is described with free-energy based lattice Boltzmann multiphase model, and the fluid-structure boundary is implemented in the form combining LBM and finite difference method (FDM). Except the obvious and traditional phenomenon such as large interface deformation and velocity variation, it has been found that the gravity-driven spherical bubble finally become a bubble ring after the coupling process. Combining the intrinsically microscopic property of LBM, the complex coupling process is researched with deeper study on relative size and fluid properties. The results may not only advance the LBM application in multiphase coupling field, but make a significant insight into the micro-transient phenomena of bubbles interacting with particles.

Keywords: Bubble, Particle, Lattice Boltzmann method
I-INCE Classification of Subjects Number(s): 21.6

1. INTRODUCTION

Due to the existence of solid boundary nearby the bubble, the bubble motion and deformation may be more complex and interesting (1). Understanding that bubble dynamics can be quite valuable in the areas such as underwater noise, structure vibration, or even explosion shock and cavitations damage (2-4). Though for the variety of solid boundary, the interaction between bubbles with different boundary conditions is widely researched, a large part of it is focused on the plane and infinite walls (5). Nevertheless, in a gas-liquid-solid mixture, the microscopical bubble is strongly influenced by the surrounding particles. Mileva E. (6) researched the hydrodynamic interaction of a solid particle and boundary layer around a rising bubble. Yoon R. (7) studied the effects of hydrodynamic and surface forces on the interaction of bubble and particles.

The lattice Boltzmann method is a rapidly developed numerical method in both single-phase flows and multi-phase flows in recent years. The method predicts the fluid behavior by solving the Navier-Stokes equations. Specially, for a multi-phase model, an additional equation is adopted to capture the interface (8, 9). An another focus of attention is the effective lattice discreteness of a body force in using LBM. Of varied schemes, that provided by Guo Z. (10) is one most effective scheme. Combining this scheme, Zheng H. et al. (9) introduced the surface tension as a body force in the multi-phase model which is based on the free-energy model. Coming up next, Zheng H. et al. (11) expanded the two-dimensional multi-phase model into a three dimensional model using different lattice velocity model for two lattice Boltzmann equations. On this foundation some novel and interesting multi-phase physics are investigated. Huang H. et al. (12) simulated one bubble rising process under different Reynolds numbers. Cheng M. et al. (13) studied

[1] shidongyan@hrbeu.edu.cn
[2] zhikai.wa@gmail.com
[3] amanzhang@gmail.com

multiple bubbles rising under gravity in a quiescent viscous incompressible fluid. Ghosh S. et al. (14) studied the rayleigh-taylor instability and bubble dynamics from a view of real physical parameters. In the simulation of bubble interaction with spherical particles, the fluid-structure boundary treatment is also an issue worthy of remark. To be not less than the precision of the whole lattice Boltzmann model, the second order accuracy must be satisfied (15, 16).

In this paper, a lattice Boltzmann multi-phase model based on the free-energy scheme and a modified bounce back scheme (17) combining the finite difference method in dealing with the solid boundary at a mesoscopic level are combined together. Taking this as the model, both the fluid property and the relative position effecting on the interaction are investigated. Furthermore, under a certain condition of fluid property, the further research of the influence of relative size is developed.

2. FORMULATION AND NUMERICAL METHOD

2.1 Lattice Boltzmann Method

The traditional lattice Boltzmann equation considering the body force can be written as (10)

$$\partial f_i / \partial t + \mathbf{e}_i \cdot \nabla f_i = \Omega_i + F_i \tag{1}$$

where *i* stands for the discrete direction. f_i is the number density distribution function in the *i* direction. $\mathbf{e}_i$ is the microscopic velocity in the *i* direction. Ω_i is the non-linear collision term which can be approximately replace by a linear term (18),

$$\Omega_i = 1/\omega \cdot (f_i^{eq} - f_i). \tag{2}$$

ω is the relaxation time parameter. f_i^{eq} is the equilibrium distribution function (EDF) which is relative to the lattice structure. For D3Q19 model used here, the EDF is chosen to be

$$\begin{cases} f_i^{eq}(\rho,\mathbf{u}) = t_i \cdot \left\{ Q_i + \rho \cdot [(\mathbf{e}_i \cdot \mathbf{u})/c_s^2 + \mathbf{uu} : (\mathbf{e}_i\mathbf{e}_i - c_s^2\mathbf{I})/(2c_s^4)] \right\} \\ Q_0 = 3\rho - 6(\phi\mu_\phi + c_s^2\rho) \\ Q_{1\sim18} = (3\rho - Q_0)/2 \end{cases} . \tag{3}$$

u is the macroscopic velocity, and c_s is the lattice sound velocity, $c_s = 1/\sqrt{3}$. t_i is the weighting factor, $t_0 = 1/3$, $t_{1\sim6} = 1/18$, $t_{7\sim18} = 1/36$. ϕ and μ_ϕ are two parameters related to the multi-phase interface capture, and a detailed introduction will be given in the next section.

F_i is a discrete body force in the micro-velocity direction. In 2002, Guo. Z. (10) provide an effective form, which gives

$$F_i = t_i \cdot (1 - 1/2\omega) \cdot \left[(\mathbf{e}_i - \mathbf{u})/c_s^2 + \mathbf{e}_i \cdot (\mathbf{e}_i \cdot \mathbf{u})/c_s^4 \right] \cdot F . \tag{4}$$

and *F* is the macro-body force.

By multi-scale expansion, and the following constrains,

$$\begin{cases} \sum_i f_i^{(0)} = \rho \\ \sum_i f_i^{(0)} \mathbf{e}_i = \rho\mathbf{u} \\ \sum_i f_i^{(0)} e_{i\alpha} e_{i\beta} = (\phi\mu_\phi + c_s^2\rho) + \rho u_\alpha u_\beta \end{cases} . \tag{5}$$

Eq. (1) can recover the Navier-Stokes with second-order precision.

2.2 Multiphase Interface Treatment

The interface movement of two phases composed of the liquid phase, ρ_l = 1000, and the gas phase, $\rho_g = 1$, is predicted by using a diffusion interface approach. The evolution process can be expressed as (9)

$$\partial\phi/\partial t + \nabla \cdot (\phi\mathbf{u}) = \theta \cdot \nabla^2 \mu_\phi . \tag{6}$$

ϕ is the defined order parameter. θ is the mobility, and μ_ϕ is the chemical potential. Instead of discrete operation, a modified lattice Boltzmann equation(19) is adopted to solve Eq. (6),

$$g_i(\mathbf{x}+\mathbf{e}_i\cdot\delta_t,t+\delta_t)=g(\mathbf{x},t)+1/\tau(g_i^{eq}(\mathbf{x},t)-g_i(\mathbf{x},t))+(1-q)(g_i(\mathbf{x}+\mathbf{e}_i\cdot\delta_t,t)-g_i(\mathbf{x},t)). \quad (7)$$

g_i is another number density distribution for the order parameter ϕ. τ is the corresponding relaxation parameter related to q, $q=1/(\tau+0.5)$. θ can be calculated, $\theta=-1/2(q-2\tau q^2)\Gamma\delta_t$. Γ is a control parameter. The chemical potential μ_ϕ can be derived from the free energy density function (20),

$$\begin{cases}\mu_\phi=A(4\phi^3-4\phi^{*2}\phi)-k\nabla^2\phi\\ k=A(W^2\phi^{*2})/2\\ A=3\sigma/(4W\phi^{*4})\end{cases}, \quad (8)$$

where W is the interface thickness, and σ is the surface tension. The order parameter ϕ^* equals to $(\rho_l-\rho_g)/2$. For the D3Q7 model is enough to recover the Cahn-Hilliard equation which does not require the fourth-order isotropic lattice tensor (11). Based on three constrains on zero, first and second moments of the equilibrium distribution, the equilibrium distribution function can be written as (11)

$$\begin{cases}g_0^{(eq)}=-3\Gamma\mu_\phi+\phi+(\phi\mathbf{e}_i\mathbf{u})/2q\\ g_{1\sim18}^{(eq)}=g_0^{(eq)}+7\Gamma\mu_\phi/2-\phi\end{cases}. \quad (9)$$

2.3 Solid Boundary Treatment

As the spherical particle is stationary, the real boundary velocity can be assumed to be zero, and the simplified expression for $f_{\tilde{i}}$ coming from the solid boundary can be written as (17)

$$f_{\tilde{i}}(\mathbf{x},t+\delta_t)-f_i^{(eq)}(\mathbf{x},t)=-t_i\rho(\mathbf{e}_i\cdot(\eta\mathbf{u}_1+(2-\eta)\mathbf{u}_2))/c_s^2. \quad (10)$$

η is the coefficient connected with numerical stability, $\eta=1-\Delta$. Δ is a parameter determined by the position where the real boundary crossing with the lattice link. Assuming $\mathbf{x}_1$ is the solid node position nearest to the real wall, $\mathbf{x}_s$ and $\mathbf{x}_2$ stand for the neighboring solid node and the fluid node in i and $\tilde{i}$ directions, respectively. Then Δ can be expressed as $\Delta=|\mathbf{x}_s-\mathbf{x}_w|/|\mathbf{x}_1-\mathbf{x}_s|$, and $\mathbf{u}_1$, $\mathbf{u}_2$ can be calculated by

$$\begin{cases}\mathbf{u}_1=(1-2\Delta)\mathbf{u}_{\mathbf{x}1}/(2-2\Delta)\\ \mathbf{u}_2=(1-2\Delta)\mathbf{u}_{\mathbf{x}2}/(4-2\Delta)\end{cases}. \quad (11)$$

where $\mathbf{u}_{\mathbf{x}1}$ and $\mathbf{u}_{\mathbf{x}2}$ are the macroscopic velocity at nodes $\mathbf{x}_1$ and $\mathbf{x}_2$.

3. RESULTS AND DISCUSSION

3.1 Validation

As benchmark problems, a bubble in the stational liquid and flow over circular cylinder are simulated to verify the lattice Boltzmann implement of gas-liquid and fluid-structure interfaces in the model. The state of a stable gas-liquid interface in liquid can be described by the Laplace law (12),

$$\Delta P=2\sigma/R. \quad (12)$$

A computational domain of 120*120*120 is used to test the bubbles with the radius 15, 20 and 25, respectively. Periodic boundary conditions are applied on the surrounding boundaries. The parameters are set as: $\rho_l=1000$, $\rho_g=1$, $\tau_\rho=0.6$, $\tau_\phi=0.6$. The numerical results compared with the theoretical results are shown in Table 1.

Table 1 – Verification of the Laplace Law

R	σ	ΔP (this paper)	ΔP (theory)	Err(%)
15	2.0	0.2699	0.267	1.0861
20	2.0	0.1999	0.200	0.05
25	2.0	0.1593	0.160	0.4375

Moreover, the case of flow over circular cylinder where the computational domain is 1600*400, and the

cylinder radius is 20 is simulated. The Reynolds number (Re) is 100. The obtained *Cd* and *Cl* are in Figure 1.

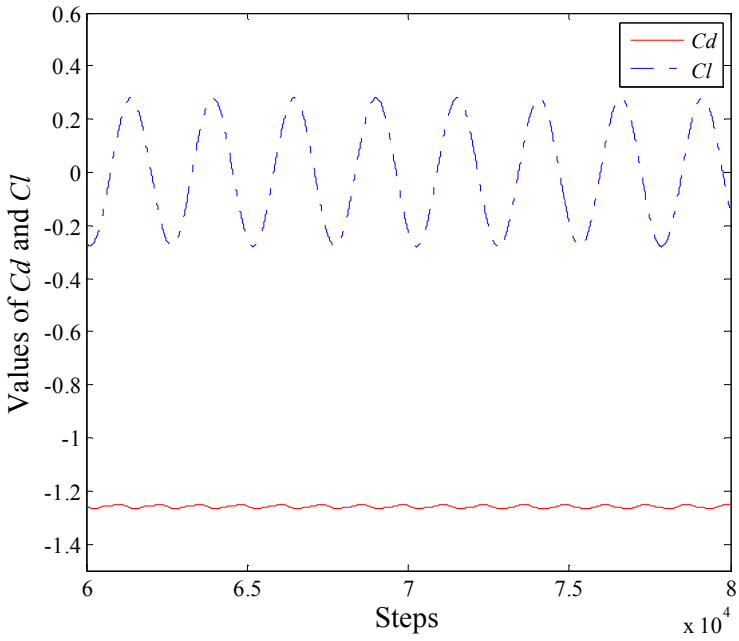

Figure 1 – Histories of the drag (*Cd*) and lift (*Cl*) coefficients

Table 1 shows that the numerical simulation values match well with the theoretical calculating results in capturing the bubble interface. The increase of inaccuracy in case 3 is caused by boundary effect of the stable computational domain. Fig. 1 shows a good handling capacity of fluid-structure boundary in the model.

3.2 Influence of Fluid Properties

The fluid properties can be defined by the following two parameters (9, 20):

$$Eo = g\Delta\rho d_b^2 / \sigma, Mo = g\Delta\rho\mu_H^4 / (\rho_H^2\sigma^3), \quad (13)$$

where g is the gravity acceleration, $\Delta\rho = \rho_H - \rho_L$, and μ_H stands for the viscosity of the liquid phase. The dimensionless time variable $t_r = \sqrt{d_b / g}$, and d_b is the diameter of the bubble.

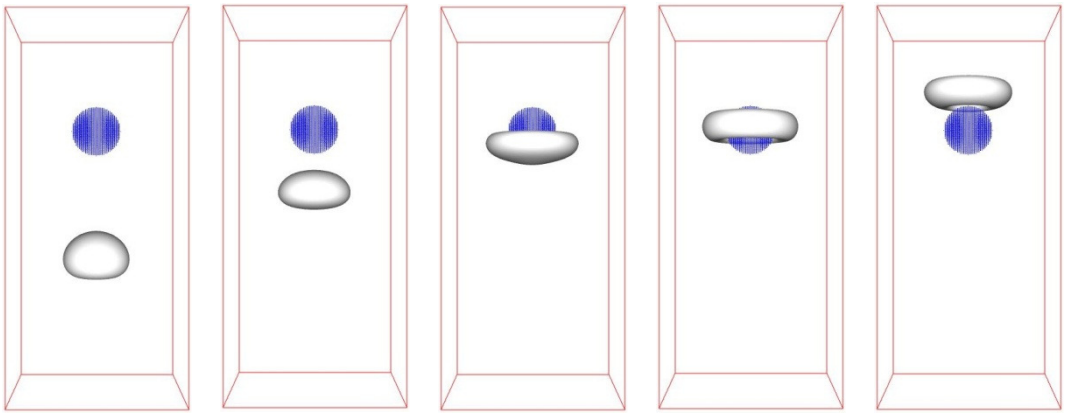

Figure 2 – Bubble rising process with an object on the trajectory path

Figure 2 shows the rising process of an bubble with an object on the trajectory path with *Eo* = 15.985, *Mo* = 1.20237. The relative size is $\beta = 0.8$. At the initial stage, the bubble rises as an isolated bubble in static flow field (11). As the bubble rises, the particle effect becomes obvious. The upper part of the bubble becomes flattened, depressed, and finally a bubble ring appears.

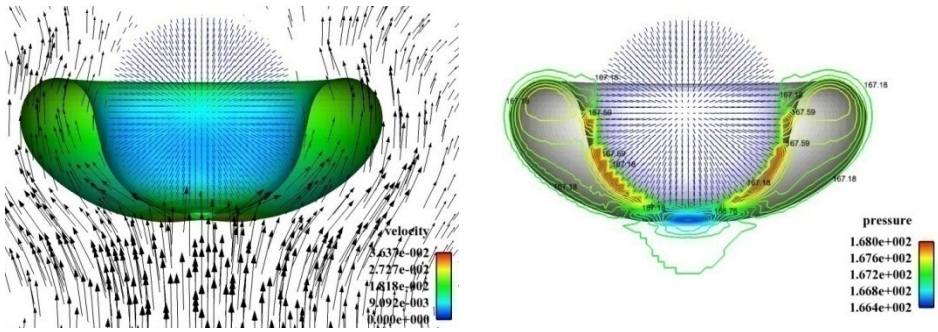

Figure 3 – At t = 7000, the (a)velocity field and (b) pressure field on bubble surface

Figure 3 is clipping views of the bubble interaction with the particle. (a) and (b) display the velocity field and the pressure field, respectively. Figure 3(a) shows the initial stage of a bubble ring appearance with an hole at the bottom of the bubble. The velocity vector suggests a jet impacting the particle. Figure 3(b) shows the corresponding pressure distribution. A low pressure area appears around the impingement hole.

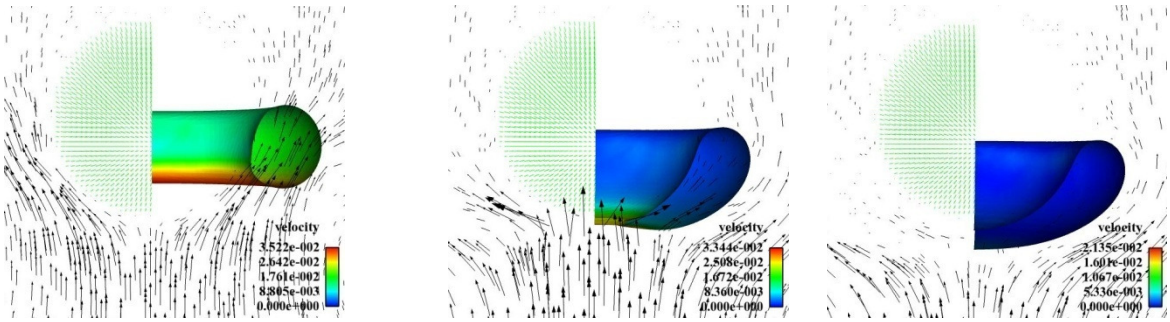

Figure 4 – At t = 8000, bubble deformation and velocity distribution under different fluid property

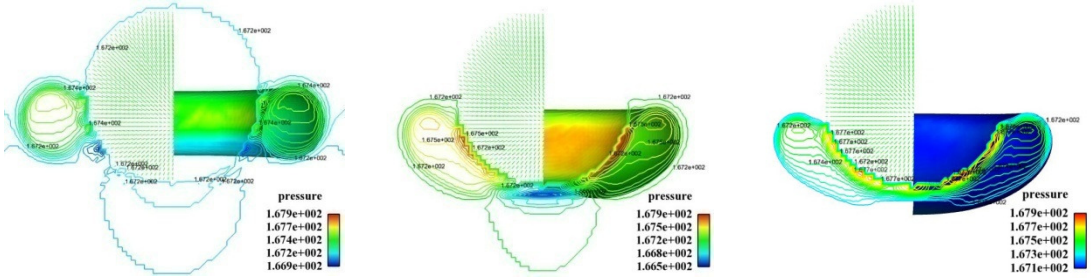

Figure 5 – At t = 8000, bubble deformation and pressure distribution under different fluid property

Keeping the value of Eo stable, the deformation, velocity and pressure distribution with $Mo = 0.49328, 1.20237, 2.49723$ are shown in Figures 4~5. A particular phenomenon that the interaction process is accelerated as the Mo decreases occurs. The bubble ring already turns up at t = 8000 with $Mo = 0.49328$, while the jet phenomenon just happens with $Mo = 1.20237$. For the larger Mo which is 2.49723, there is quite a long process before the jet happens. During the interaction, the fluid particles on the bottom part of the bubble move more faster comparing with that on the other part. Figure 4 shows that a high pressure area turns up between the bubble and the particle as the bubble approaches the solid wall. On the effect of letting out pressure when the impingement hole is formed, the pressure at the location between the bubble and the particle degrades rapidly.

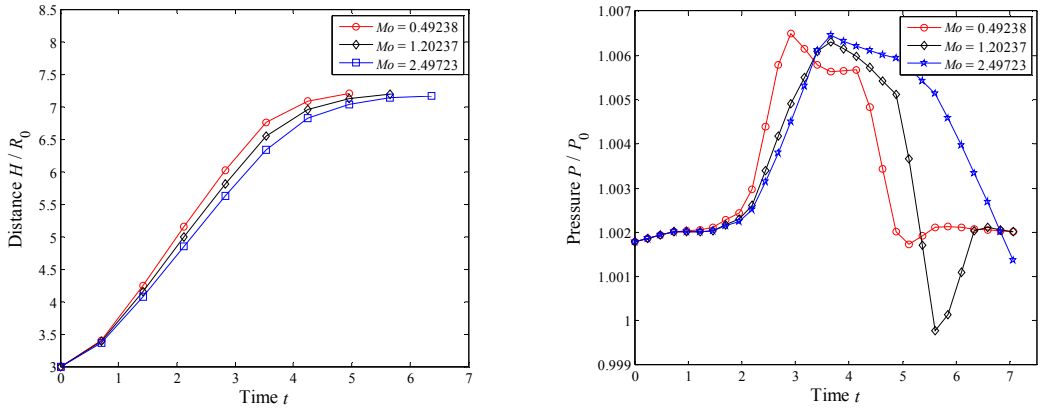

Figure 6 – Under different conditions of fluid property, (a) histories of the bubble center position; (b) histories of the pressure at node (55,55,150)

Under different conditions of fluid property, the initial position of the bubble is kept at (55,55,61). Figure 6(a) and (b) record the histories of the bubble center position and the pressure at the node (55,55,150) under the spherical particle. The nondimensional time is normalized by the parameter $t_r = \sqrt{d_b / g}$. Just as the suggestion of the three lines in Figure 6(a), the terminal position of the bubble with different *Mo* values is almost the same, however, the smaller the *Mo* is, the bigger the acceleration is. Figure 5(b) shows that when the bubble moves close to the spherical particle, the pressure of the node (55,55,150) increases rapidly. When the bubble position tends to be stable, the pressure gradually decreases, but at the jet stage, it decreases rapidly. Finishing the jet process, a bubble ring is formed and the pressure calls back. As *Mo* decreases, the response process goes more quickly.

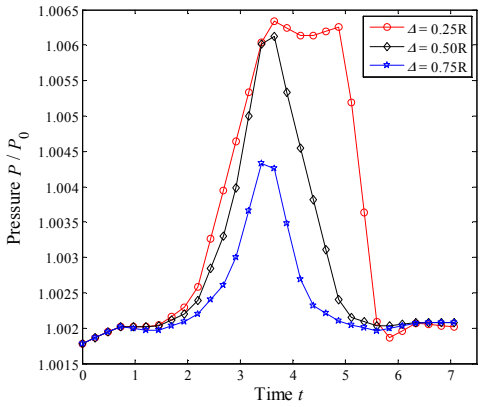

Figure 7 – Histories of the pressure at the node (55,55,150) with different values that the bubble biases the axis of the particle

Figure 7 shows the histories of the pressure at that node with different values that the bubble biases the axis of the particle keeping $Eo = 15.984$ and $\tau_\phi = 0.75$. The similar phenomenon that a rapid drop procedure sticks with a rapid rise procedure appears. However, the rapid drop procedure is not caused by the jet process, but the bubble moving away from the particle. Because an interesting phenomenon that bubble rises from the side of the particle in stand of becoming a bubble ring turns up when the bubble is not coaxial with the particle. The more the offset is, the smaller the peak value of pressure will be.

3.3 Influence of Relative Size

The effects of the relative size β ($\beta = R_p / R_b$, R_p is the radius of the particle, and R_b is the radius of the bubble) will be studied in the next. Keeping the fluid properties, the interface thickness and the surface tension fixed, the relative size is chosen as $\beta = 0.8$, 1.0, and 1.2 with $R_b = 20$.

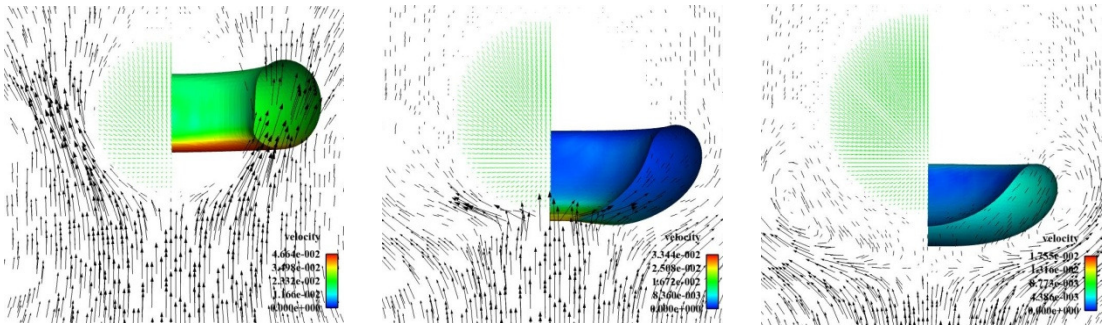

Figure 8 – At t = 8000, bubble deformation and velocity distribution for (a) $\beta = 0.8$; (b) $\beta = 1.0$; (c) $\beta = 1.2$

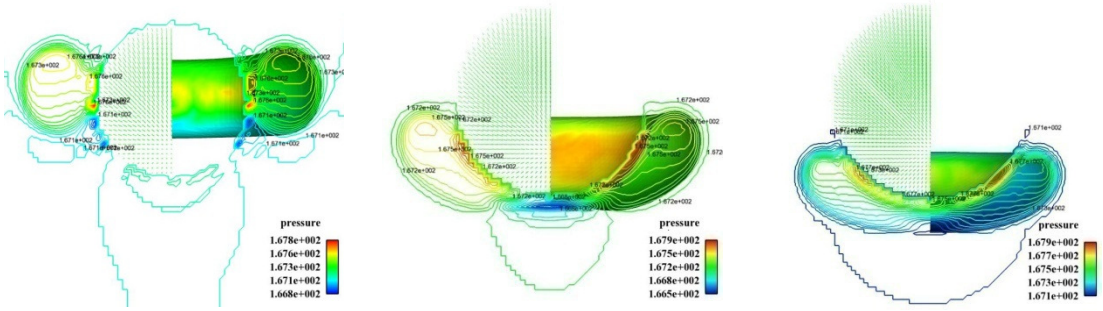

Figure 9 – At t = 8000, bubble deformation and pressure distribution for (a) $\beta = 0.8$; (b) $\beta = 1.0$; (c) $\beta = 1.2$

Figures 8 and 9 show the clipping views of the interaction process coupling with the velocity vector field and the pressure field at the key point, respectively. Compared with the other two cases, a bubble ring already generated at t = 8000 for $\beta = 0.8$. while the other two cases are still in the jet stage for $\beta = 1.0$, and the extrusion stage for $\beta = 1.2$. By comparative analysis, it can be found that the fastest-coupling velocity for $\beta = 0.8$. The it can be concluded that both decreasing *Mo* and decreasing particle size can improve the interaction process and speed up forming a bubble ring. It can also be found that great differences in the property of velocity and pressure around the bubble exist. During the interaction, the velocity of the upper surface of the bubble is faster the that of the bottom, and the pressure on the surface adjacent to the solid wall is higher than the other parts due to the extrusion process.

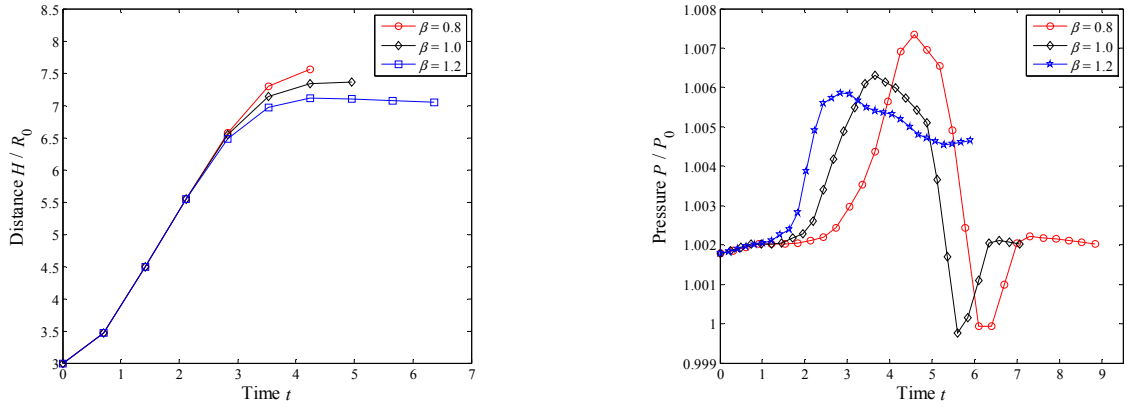

Figure 10 – With different relative size, $\beta = 0.8,1.0,1.2$, (a) histories of the bubble center position; (b) histories of the pressure at nodes (55,55,154), (55,55,150), (55,55,146)

The histories of the bubble center position and the pressure at nodes (55,55,154), (55,55,150), (55,55,146) are shown in Figure 10. The nodes detecting the pressure are chosen according to the particle size that are the nearest fluid node adjacent to the solid wall. Figure 10(a) shows that the trend is merely influenced by the relative size, but the terminal position is affected due to the position of the solid wall. Figure 10(b) shows that the smaller the particle is , the larger the maximum pressure will be.

The rapid drop and correction process induced by the jet is also suggested in Figure 10(b).

4. CONCLUSION

To investigate the interaction between bubbles and its surrounding particles in the gas-liquid-solid mixture, a three-dimensional model of bubble interaction with spherical particle is developed using the lattice Boltzmann method. Both the fluid property, relative position and the relative size effecting the interaction process are studied. The following conclusions are drawn:

(1) When the bubble is coaxial with the particle, a spherical bubble will translate into a bubble ring during the interaction, but the bubble will rise from the side of the particle when it is not coaxial with the particle.

(2) A pressure evolution that the pressure firstly increases rapidly, and then decreases via the slow stage and the rapid stage with a correction process at last is observed for the fluid node under the particle. As *M*o decreases, the response process goes more quickly.

(3) When the bubble is not coaxial the particle, the more the offset is, the smaller the peak value of pressure for the fluid node under the particle will be.

(4) When the bubble is coaxial with the particle, the smaller the particle is , the larger the maximum pressure will be.

ACKNOWLEDGEMENTS

This paper is funded by the International Exchange Program of Harbin Engineering University for Innovation-oriented Talents Cultivation.And the authors are grateful to the Program of the Scientists Fund for Outstanding Young Scholars of China (Grant No. 51222904) and the Program for New Century Excellent Talents in University (Grant No. NCET100054) for support.

REFERENCES

1. Popinet S, Zaleski S. Bubble collapse near a solid boundary: a numerical study of the influence of viscosity. J Fluid Mech. 2002; 464: 137-163.
2. Ji B, Luo X, Peng X. Numerical analysis of cavitation evolution and excited pressure fluctuation around a propeller in non-uniform wake. Int J Multiphas Flow. 2012; 43: 13-21.
3. Zhang A, Ni B, Song B. Numerical simulation of bubble breakup phenomena in a narrow flow field. Appl Math Mech-Engl. 2010; 31: 449-460.
4. Zhang AM, Wang SP, Wu GX. Simulation of bubble motion in a compressible liquid based on the three dimensional wave equation. Eng Anal Bound Elem. 2013; 37(9): 1179-1188.
5. Vogel A, Lauterborn W, Timm R. Optical and acoustic investigations of the dynamics of laser-produced cavitation bubbles near a solid boundary. J Fluid Mech . 1989; 206: 299-338.
6. Mileva E. Solid particle in the boundary layer of a rising bubble. Colloid Polym Sci. 1990; 268(4): 375-383.
7. Yoon RH. The role of hydrodynamic and surface forces in bubble–particle interaction. Int J Miner Process. 2000; 58(1): 129-143.
8. Ohta M, Sussman M. The buoyancy-driven motion of a single skirted bubble or drop rising through a viscous liquid. Phys Fluids. 2012; 24(11): 112101.
9. Zheng HW, Shu C, Chew YT. Lattice Boltzmann interface capturing method for incompressible flows. Phys Rev E. 2005; 72(5): 056705.
10. Guo Z, Zheng C, Shi B. Discrete lattice effects on the forcing term in the lattice Boltzmann method. Phys Rev E. 2002; 65(4): 046308.
11. Zheng HW, Shu C, Chew YT, et al. Three‐dimensional lattice Boltzmann interface capturing method for incompressible flows. Int J Numer Meth Fl. 2008; 56(9): 1653-1671.
12. Huang H, Zheng H, Lu X. An evaluation of a 3D free‐energy‐based lattice Boltzmann model for multiphase flows with large density ratio. Int J Numer Meth Fl. 2010; 63(10): 1193-1207.
13. Cheng M, Hua J, Lou J. Simulation of bubble–bubble interaction using a lattice Boltzmann method. Comput Fluids. 2010; 39(2): 260-270.
14. Ghosh S, Das AK, Vaidya AA. Numerical study of dynamics of bubbles using lattice Boltzmann method. Ind Eng Chem Res. 2012; 51(18): 6364-6376.
15. Mei R, Shyy W, Yu D. Lattice Boltzmann method for 3-D flows with curved boundary. J Comput Phys. 2000; 161(2): 680-699.
16. Wu J, Shu C. An improved immersed boundary-lattice Boltzmann method for simulating three-dimensional incompressible flows. J Comput Phys. 2010; 229(13): 5022-5042.

17. Shi DY, Wang WZ, Zhang AM. A novel lattice Boltzmann method dealing with arbitrarily complex fluid-solid boundaries. Acta Phys Sin. 2014; 63(7): 074703.
18. Bhatnagar PL, Gross EP, Krook M. A model for collision processes in gases. I. Small amplitude processes in charged and neutral one-component systems. Phys Rev. 1954; 94(3): 511.
19. Qian YH, d'Humières D, Lallemand P. Lattice BGK models for Navier-Stokes equation. EPL (Europhysics Lett). 1992; 17(6): 479.
20. Zheng HW, Shu C, Chew YT. A lattice Boltzmann model for multiphase flows with large density ratio. J Comput Phys. 2006; 218(1): 353-371.